CrystEngComm

PAPER

View Article Online
View Journal | View Issue

Cite this: *CrystEngComm*, 2025, **27**, 6462

Design of a new nitronyl-nitroxide biradical and its complexes: synthesis, crystal structures and magnetic properties†

Cristian Andrei Spinu,[ab] Ghenadie Novitchi,[c] Mihaela Hillebrand,[a] Teodora Mocanu,[d] Gabriela Ionita,[d] Anamaria Hanganu,[b] Victoriţa Tecuceanu[b] and Marius Andruh *[ab]

Received 14th August 2025,
Accepted 9th September 2025

DOI: 10.1039/d5ce00795j

rsc.li/crystengcomm

A new nitronyl-nitroxide biradical, H_2L, has been obtained starting from bisphenol A, through successive nitration, formylation, and Ullman reactions. Using this molecule as a ligand, two isostructural binuclear complexes. $(Et_3NH)_2[Co_2L(hfac)_4]\cdot CHCl_3$ **1** and $(Et_3NH)_2[Ni_2L(hfac)_4]\cdot CHCl_3$ **2**, have been synthesized and characterized by single crystal X-ray diffraction. Their magnetic properties have been investigated and revealed relatively strong antiferromagnetic interactions between the metal ions and the nitronyl-nitroxide moieties.

Introduction

Nitronyl-nitroxides (NN), stable and persistent radicals (Scheme 1), are useful ingredients for designing molecular magnetic materials.[1] These molecules can act as ligands towards paramagnetic 3d and 4f metal ions, generating heterospin complexes with ferro- and antiferromagnetic interactions between the spin carriers varying between large limits. The interplay between the strong couplings and the magnetic anisotropy, the last one brought by the metal ions, leads to families of compounds with exciting magnetic properties: molecular nanomagnets (single molecule magnets, SMM, and single chain magnets, SCM), which are of high interest for applications in data storage. The first single chain magnet, reported in 2001 by Gatteschi *et al.*,[2] is a coordination polymer constructed from cobalt(II) nodes bridged by a nitronyl-nitroxide ligand. SCMs characterized by high coercive fields,[3a,b] or by a high blocking temperature (15.5 K)[3c] are also cobalt(II) coordination polymers with nitronyl-nitroxide bridging ligands.

These organic radicals are readily obtained from aldehydes following or adapting Ullman's synthetic protocol.[4] The nitronyl-nitroxide platform can be decorated with various coordinating groups, arising from the starting formyl derivatives. The richness of the nitronyl-nitroxide class of ligands is directly related to the availability of various aldehyde precursors. Indeed, the need for these molecules as ligands continuously stimulates the design of new aldehydes functionalized with coordinating groups. Moreover, starting from polyladehydes, polyradicals can be synthesized as well. For example, ligands with two nitronyl nitroxide units in *meta* position on the same phenyl ring led to mononuclear and homometallic polynuclear metal complexes containing Mn^{II},[5] Cu^{II},[6] Y^{III},[7] Pr^{III},[8] Nd^{III},[8,9] Sm^{III},[8] Gd^{III}, Tb^{III}, Dy^{III},[7–10] Ho^{III},[7] as well as to heterometallic complexes: Ln^{III}–Mn^{II} (where Ln: Gd, Dy),[11,12] Ln^{III}–Co^{II} (where Ln: Gd, Tb, Dy, Ho),[13] Ln^{III}–Ni^{II} (where Ln: Tb, Dy),[12] Ln^{III}–Cu^{II} (where Ln: Gd, Tb, Dy, Ho, Y),[14–16] and Dy^{III}–Zn^{II}.[17] Ligands with two nitronyl-nitroxide units in *para* position on the same benzenic ring led to both mononuclear complexes and coordination polymers containing Cu^{II},[6a,18] Mn^{II},[19] Y^{III}, Gd^{III}, Tb^{III}, and Dy^{III},[20] metal ions.

Other families of biradicals are characterized by larger distances between the two NN groups, which are attached onto different fragments within the same molecule. The structures of several compounds are depicted in Scheme 2. For example, the two ligands derived from 2,2′-bipyridine (**I**

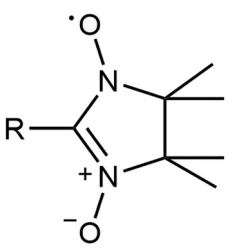

Scheme 1 Nitronyl-nitroxide radical.

[a] *Faculty of Chemistry, University of Bucharest, Regina Elisabeta Blvd. 4-12, Bucharest, 030018, Romania. E-mail: marius.andruh@acad.ro*
[b] *C. D. Nenitzescu Institute of Organic and Supramolecular Chemistry of the Romanian Academy, Splaiul Independentei, 202B, 060023, Bucharest, Romania*
[c] *CNRS, University Grenoble Alpes, LNCMI, F-38000 Grenoble, France*
[d] *"Ilie Murgulescu" Institute of Physical Chemistry, Romanian Academy, Bucharest, Romania*

† This paper is dedicated to Professor Eva Rentschler, on the occasion of her 60th birthday.

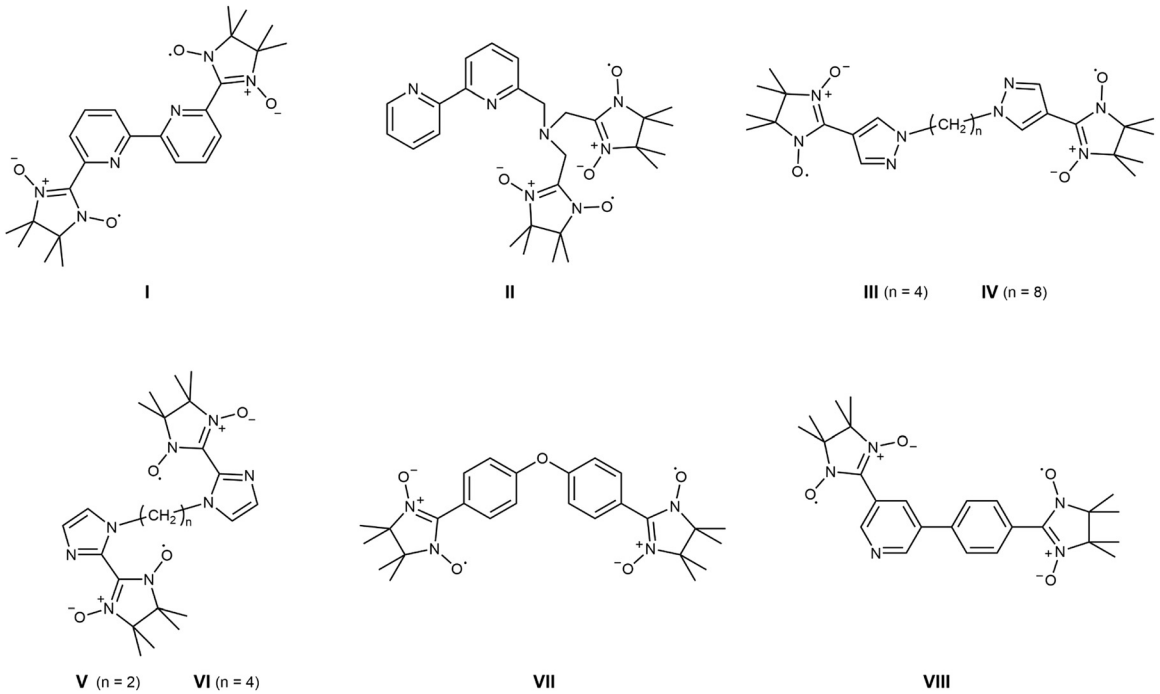

Scheme 2 Nitronyl-nitroxide biradicals.

and **II**) generate mononuclear complexes with 3d metal ions.[21,22] The ligands **III** and **IV**, with NN fragments separated by 4 or 8 methylene groups, led to 1D and 2D coordination polymers with Cu^{II} nodes.[23] For the biradicals **V** and **VI**, with NN groups attached to imidazole rings separated by 2 or 4 methylene groups, chains and binuclear complexes of Gd^{III}, Tb^{III}, and Dy^{III} have been obtained and characterized.[24] The biradical derived from di-phenyl-ether **VII** led to a 2D coordination polymer of Cu^{II},[25] while the one derived from 5-phenyl-3-pyridyl **VIII** generates an octanuclear Cu^{II} complex and Ln^{III}–Cu^{II} chains (where Ln: Gd, Tb, Dy).[26]

In this paper we report on the synthesis of a new nitronyl nitroxide biradical (Scheme 3) derived from bisphenol A, and on the crystal structures and magnetic properties of two dinuclear complexes generated by this ligand: $(Et_3NH)_2[M^{II}_2\text{-}L(hfac)_4]\cdot CHCl_3$, where M: Co, Ni.

Experimental

Materials and methods

The 2,3-bis(hydroxylamino)-2,3-dimethylbutan,[27] 4,4′-(propane-2,2-diyl)bis(2-nitrophenol),[28] were synthesized as previously described. Silica gel used in column chromatography was silica gel 60 (0.062–0.200 mm) from Merck. All other reagents and solvents were commercially purchased and used without any further purification, if not stated otherwise.

Synthesis

Synthesis of 5,5′-(propane-2,2-diyl)bis(2-hydroxy-3-nitrobenzaldehyde). The synthesis of the dialdehyde was devised and adapted from reported procedures on similar compounds.[29]

Method (a). 4,4′-(Propane-2,2-diyl)bis(2-nitrophenol) (1.000 g, 3.142 mmol, 1 eq.) and hexamethylenetetramine (1.762 g, 12.568 mmol, 4 eq.) were dissolved in 10 mL of CF_3COOH under nitrogen and refluxed for 4 days. The reaction was monitored daily by TLC. Then, after cooling the solution, 10 mL of 3 M HCl solution were added and refluxed for 1 hour. After cooling, the solution was extracted two times with 25 mL of $CHCl_3$, and the combined organic phases were washed with 50 mL of 3 M HCl solution, 50 ml of H_2O and then dried over $MgSO_4$.

After evaporation of the solvent under vacuum a crude yellow-orange solid was obtained. The crude solid was dissolved in minimum amount of $CHCl_3$ and purified by column chromatography using silica gel, as stationary phase, using as eluents $CHCl_3$ for the starting material, a mixture of $CHCl_3$: ethyl acetate = 19 : 1 (v : v) for the monoaldehyde and a gradient from $CHCl_3$: ethyl acetate = 19 : 1 (v : v) to $CHCl_3$: ethyl acetate = 1 : 1 (v : v) for the dialdehyde. The eluate was collected as 50 mL fractions and products were identified by TLC, hexane : $CHCl_3$ = 9 : 1 (v : v) with R_f = 0.8 for monoaldehyde and R_f = 0.4 for dialdehyde. The monoaldehyde fractions were evaporated and the solid dissolved in ethyl acetate then, the obtained solution was let to evaporate to obtain the monoaldehyde as a light yellow powder 0.456 g, yield 42%. The dialdehyde fractions were evaporated under vacuum and the solid dissolved in hot ethyl acetate, the obtained solution was let to evaporate to obtain an orange-yellow solid which was washed carefully with small amounts of ice-cold ethyl acetate, filtered and dissolved again

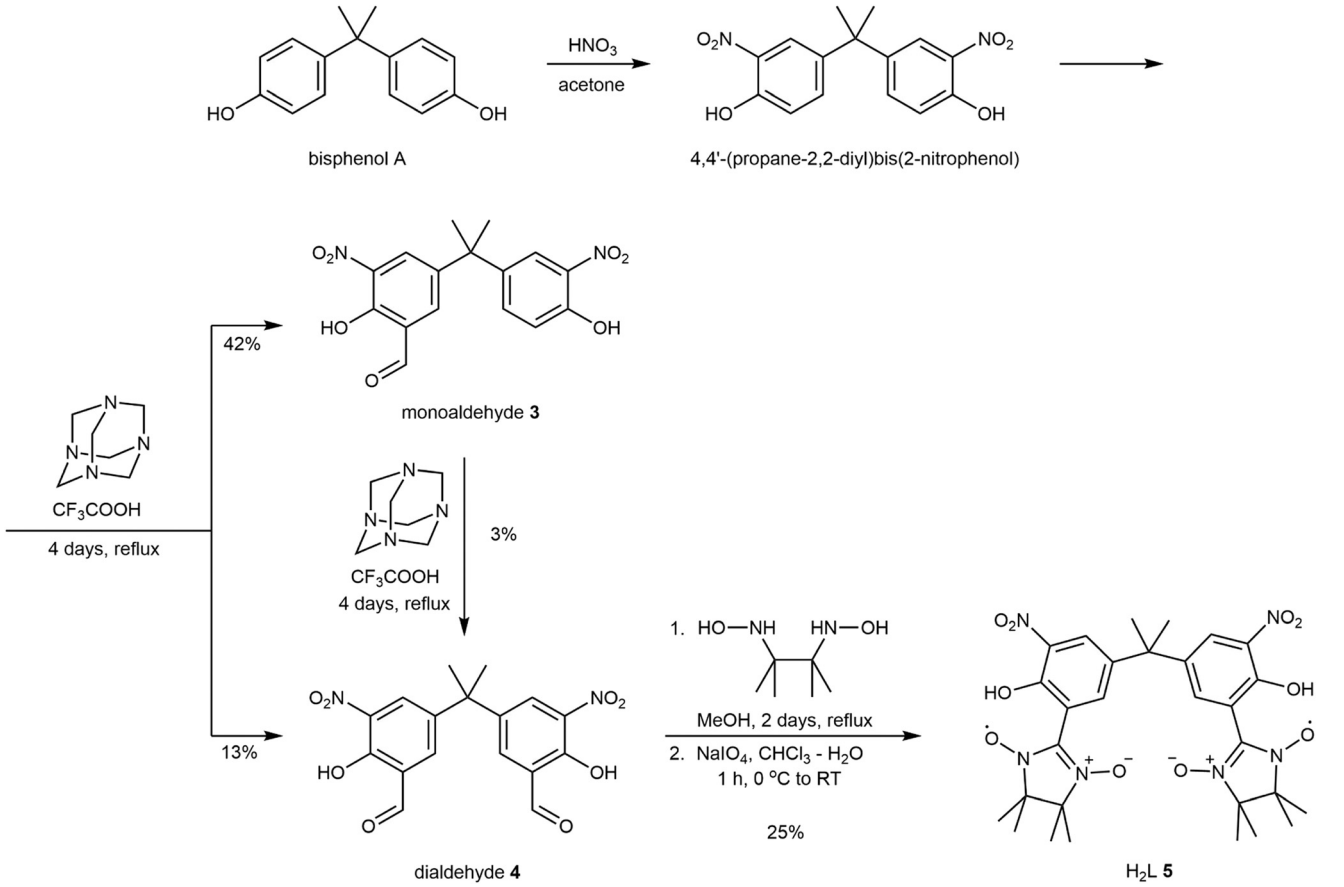

Scheme 3 Synthesis of monoaldehyde **3**, dialdehyde **4** and nitronyl-nitroxide ligand H_2L **5**.

in hot ethyl acetate. Upon the slow evaporation of the solution, dialdehyde was isolated as yellow crystals 0.149 g, yield 13%.

2-Hydroxy-5-(2-(4-hydroxy-3-nitrophenyl)propan-2-yl)-3-nitrobenzaldehyde (monoaldehyde) **3**. Selected IR peaks (cm^{-1}): 3294 (m), 2966 (w), 2920 (w), 2876 (w), 1695 (vs), 1626 (s), 1589 (m), 1572 (m), 1539 (vs), 1462 (s), 1421 (s), 1408 (s), 1371 (s), 1348 (s), 1327 (vs), 1306 (vs), 1258 (vs), 1180 (s), 1157 (s), 1140 (m), 1107 (m), 1079 (w), 972 (w), 930 (m), 895 (w), 837 (w), 824 (w), 783 (w), 768 (w), 728 (w), 704 (m), 660 (m), 629 (w), 617 (w), 586 (m), 567 (w), 548 (w), 465 (w), 423 (w), 441 (w). ^{1}H-NMR (500.13 MHz, $CDCl_3$, δ ppm, J Hz): 11.27 (s, 1H, OH), 10.53 (s, 1H, OH), 10.38 (s, 1H, CHO), 8.20 (d, 1H, H_{Ar}, 2.6 Hz), 8.03 (d, 1H, H_{Ar}, 2.5 Hz), 7.93 (d, 1H, H_{Ar}, 2.6 Hz), 7.32 (dd, 1H, H_{Ar}, 2.5 Hz, 8.8 Hz), 7.09 (d, 1H, H_{Ar}, 8.8 Hz), 1.73 (s, 6H, CH_3) ppm. ^{13}C-NMR (500.13 MHz, $CDCl_3$, δ ppm): 188.86, 154.97, 153.82, 141.64, 140.79, 136.46, 135.15, 134.85, 133.12, 128.78, 125.43, 121.97, 120.51, 42.16, 30.28 ppm. MS (−ESI): [M−H] = 345.1 (m/z) (exact mass 346.08).

5,5′-(Propane-2,2-diyl)bis(2-hydroxy-3-nitrobenzaldehyde) (dialdehyde) **4**. Selected IR peaks (cm^{-1}): 3144 (w), 3092 (w), 3042 (w), 2978 (m), 2939 (w), 2880 (w), 2760 (w), 2662 (w), 2581 (w), 1695 (s), 1672 (vs), 1663 (vs), 1620 (m), 1595 (m), 1537 (vs), 1528 (vs), 1462 (s), 1422 (m), 1393 (m), 1373 (vs), 1348 (s), 1310 (s), 1294 (m), 1271 (vs), 1250 (s), 1217 (s), 1175 (m), 1159 (m), 1123 (w), 1109 (w), 1013 (w), 966 (m), 951 (m), 924 (w), 910 (w), 878 (w), 791 (m), 770 (m), 733 (m), 689 (w), 646 (w), 629 (w), 596 (w), 579 (w), 469 (w). ^{1}H-NMR (500.13 MHz, $CDCl_3$, δ ppm, J Hz): 11.26 (s, 2H, OH), 10.39 (s, 2H, CHO), 8.21 (d, 2H, H_{Ar}, 2.6 Hz), 7.91 (d, 2H, H_{Ar}, 2.6 Hz), 1.76 (s, 6H, CH_3) ppm. ^{13}C-NMR (500.13 MHz, $CDCl_3$, δ ppm): 188.59, 155.19, 140.80, 134.98, 134.86, 128.68, 125.67, 42.34, 30.29 ppm. MS (−ESI): [M−H] = 373.1 (m/z) (exact mass 374.08).

Method (b). 2-Hydroxy-5-(2-(4-hydroxy-3-nitrophenyl) propan-2-yl)-3-nitrobenzaldehyde (monoaldehyde) **3** (1.000 g, 2.888 mmol, 1 eq.) and hexamethylenetetramine (1.619 g, 11.551 mmol, 4 eq.) were dissolved in 10 mL CF_3COOH under nitrogen and refluxed for 4 days. The reaction work-up and purification are the same as described in method (a). The dialdehyde was isolated as yellow crystals 0.035 g, yield 3%.

Synthesis of 2,2′-(propane-2,2-diylbis(6-hydroxy-5-nitro-3,1-phenylene))bis(4,4,5,5 tetramethyl-4,5-dihydro-1*H*-imidazole-1-oxyl-3-oxide) (H_2L) 5. The synthesis of the nitronyl-nitroxide radical was adapted from previous reported procedures.[4,27]

5,5′-(Propane-2,2-diyl)bis(2-hydroxy-3-nitrobenzaldehyde) (dialdehyde) (0.485 g, 1.297 mmol, 1 eq.) and 2,3-bis(hydroxylamino)-2,3-dimethylbutan (0.422 g, 2.853

mmol, 2.2 eq.) were dissolved in 30 mL of methanol and refluxed for 48 h. After cooling, the methanol was evaporated under vacuum and solid obtained was dissolved in 30 mL of $CHCl_3$ and placed in an ice bath. Over, was added a solution of $NaIO_4$ (0.555 g, 2.594 mmol) in 30 mL of H_2O and the reaction was let to evolve 30 minutes under the ice bath and 30 minutes at room temperature. The organic phase was separated and washed with 30 mL of H_2O and dried over $MgSO_4$ followed by the evaporation of the solvent under vacuum. The crude product was purified by column chromatography, using silica-gel as stationary phase, with the elution system with a gradient, starting from pure $CHCl_3$ to $CHCl_3$: ethyl acetate = 9 : 1 (v : v) to $CHCl_3$: ethyl acetate = 1 : 1 (v : v). The product was identified in the blue coloured fractions by TLC, hexane : $CHCl_3$ = 8 : 2 (v : v) with R_f = 0.4. The solvent was evaporated and the solid was suspended in a small amount of cold ethyl acetate, filtered, washed with small amounts of cold ethyl acetate and air dried to obtain the radical as a blue powder 0.204 g, yield 25%. Selected IR peaks (cm^{-1}): 3447 (w), 3082 (w), 2976 (w), 2941 (w), 2876 (w), 2725 (w), 2598 (w), 1736 (w), 1618 (w), 1582 (w), 1537 (vs), 1472 (m), 1450 (m), 1415 (w), 1393 (m), 1371 (s), 1339 (m), 1279 (m), 1215 (w), 1161 (m), 1134 (m), 1105 (w), 976 (w), 924 (w), 893 (w), 872 (w), 816 (w), 789 (w), 766 (w), 714 (w), 687 (w), 662 (w), 598 (w), 542 (w), 459 (w). UV-vis (nm): 399, 578. MS (+ESI and −ESI): [M + H] = 629.2 (*m*/*z*) and [M–H] = 627.2 (*m*/*z*) (exact mass 628.25).

Synthesis of $(Et_3NH)_2[Co_2L(hfac)_4]\cdot CHCl_3$ 1. $Co(hfac)_2\cdot 2H_2O$ (0.0356 g, 0.0700 mmol, 2 eq.) was dissolved in 10 mL of heptane and refluxed for 30 min. Then, after cooling down the solution, another 15 mL of $CHCl_3$ solution containing H_2L (**5**) (0.0220 g, 0.0350 mmol, 1 eq.) and triethylamine (0.0073 g, 0.0717 mmol, 10 μL, 2.05 eq.) was added over. The solution was refluxed for 30 min, cooled down and filtered. After allowing the solvent to slowly evaporate for three days, brown-red crystals of the product were obtained 0.0172 g, yield 26%. Selected IR peaks (cm^{-1}): 3435 (w), 2992 (w), 2893 (w), 2673 (w), 2500 (w), 1649 (m), 1618 (w), 1553 (m), 1530 (m), 1476 (m), 1396 (w), 1362 (w), 1258 (vs), 1204 (s), 1148 (vs), 1099 (w), 950 (w), 925 (w), 900 (w), 870 (w), 827 (w), 810 (w), 793 (w), 764 (w), 743 (w), 673 (m), 586 (w), 546 (w), 529 (w), 454 (w). UV-vis (nm): 410, 550, 1168.

Synthesis of $(Et_3NH)_2[Ni_2L(hfac)_4]\cdot CHCl_3$ 2. $Ni(hfac)_2\cdot 2H_2O$ (0.0356 g, 0.0700 mmol, 2 eq.) was dissolved in 10 mL of heptane and refluxed for 30 min. Then, after cooling down the solution, another 15 mL of $CHCl_3$ solution containing H_2L (0.0220 g, 0.0350 mmol, 1 eq.) and triethylamine (0.0073 g, 0.0717 mmol, 10 μL, 2.05 eq.). The solution was refluxed another 30 min, cooled down and filtered. After allowing the solvent to slowly evaporate for three days, purple-red crystals of the product were obtained 0.0135 g, yield 20%. Selected IR peaks (cm^{-1}): 3431 (w), 2993 (w), 2893 (w), 2681 (w), 2506 (w), 1645 (m), 1618 (w), 1553 (m), 1531 (m), 1475 (m), 1396 (w), 1362 (w), 1258 (vs), 1204 (s), 1148 (vs), 1096 (w), 947 (w), 924 (w), 901 (w), 870 (w), 826 (w), 808 (w), 793 (w), 764 (w), 743 (w), 669 (m), 584 (w), 546 (w), 528 (w), 457 (w). UV-vis (nm): 402, 566, 748, 1093.

Physical measurements

IR spectra were recorded on a FTIR Bruker Tensor V-37 spectrophotometer (KBr pellets) in the range of 4000–400 cm^{-1}. UV-vis diffuse reflectance spectra were recorded on a JASCO V-670 spectrophotometer on undiluted samples in the range 200–1400 nm. The X-ray powder diffraction measurements (XRPD) were carried out on a Proto AXRD Benchtop using the Cu-Kα radiation with a wavelength of 1.54059 Å in the range 5–35° 2θ. All nuclear magnetic resonance (^1H and ^{13}C NMR) measurements were recorded on a Bruker Avance III Ultrashield Plus spectrometer operating at 11.74 T, corresponding to the resonance frequency of 500.13 MHz for the ^1H nucleus at 25 °C. Chemical shifts (δ) are referenced to residual peaks of solvent ($CDCl_3$). For MS spectra Varian 310 – MS LC/MS/MS triple quadrupole mass spectrometer fitted with an electrospray ionization interface (ESI) was used. Air was used as drying gas at a pressure of 19 psi and temperature according to experiment. The nebulizing gas was nitrogen to 40 psi for positive ionization and air to 55 psi for negative ionization. The needle voltage had been established to the potential 5000 V for positive ionization and −4500 V for negative ionization. The solution was injected directly into the interface using a syringe pump Harvard 11PLUS, with a 0.010 mL min^{-1} flow. Thus, protonated or deprotonated molecular ion obtained was selected by the first quadrupole. Into the second quadrupole, the protonated or deprotonated molecular ion was fragmented by collision with an inert gas (argon) to 1.5 mTorr pressure. Fragments were analyzed by the third quadrupole. Prior to these experiments it was performed the tuning of mass spectrometer using PPG both for positive and negative. Direct current (DC) magnetic susceptibility data (2–300 K) were collected on powdered samples using a SQUID magnetometer (Quantum Design MPMS-XL), applying a magnetic field of 0.1 T. All data were corrected for the contribution of the sample holder and the diamagnetism of the samples estimated from Pascal's constants.[30–32] The field dependence of the magnetization (up to 5 T) was measured at 2.0, 3.0, 4.0 and 5.0 K. The temperature dependence of the magnetic susceptibility, as well as the field dependence of the magnetization, have been simultaneously analyzed using the PHI program.[33] The EPR spectra of H_2L **5** in toluene, dichloromethane (DCM) and water solutions were collected using Jeol FA-100 X-band spectrometer equipped with a nitrogen flow temperature control unit. The EPR parameters set for these measurements were: microwave power 1 mW, frequency 100 kHz, sweep field 100 G, center field 3217 G, sweep time 480 s, modulation width 1 G. The EPR spectra were collected at variable temperature for H_2L **5** in water in the temperature range 20–60 °C. The hyperfine coupling constants (a_N) were evaluated using WinSim software available from NIEHS.[34]

Crystal structure determination and refinement

The X-ray crystallographic data for compounds **1**, **2** and **4** were collected on a Rigaku XtaLAB Synergy, Single source at offset/far, HyPix diffractometer equipped with a graphite-monochromated Mo Kα radiation source (λ = 0.71073 Å). The structure was solved by direct methods and refined by full-matrix least squares techniques based on F^2. The non-H atoms were refined with anisotropic displacement parameters. Hydrogen atoms were introduced in fixed, idealized positions and refined using riding models. Calculations were performed using SHELXT and SHELXL-2015/2018 crystallographic software packages.[35] A summary of the crystallographic data and the structure refinement is given in Tables 1 and S1. CCDC deposition numbers are 2478210 for (**1**), 2478211 for (**2**), and 2478212 for (**4**).

Computational details

The calculations for the two fragments were performed by the broken symmetry approach in the frame of the Gaussian09 program.[36] We have considered two states, a high spin (HS) one with S = 3/2 (S = 1/2 for radical and S = 1 for the Ni^{II} ion) and a broken symmetry (BS) state with S = 1/2 (S = −1/2 for the radical and S = 1 for the Ni^{II} ion). The energy of this spin state was checked for the stability. The calculations were performed with the B3LYP functional,[37] and the lanldz2,[38] and TZVP,[39] basis sets.

Results and discussion

The synthesis of the ligand (Scheme 3) started from bisphenol A which was converted with nitric acid to 4,4′-(propane-2,2-diyl)bis(2-nitrophenol).[28] Subsequently, the nitro derivative was formylated by Duff reaction,[29] using hexamethylenetetramine and trifluoroacetic acid to obtain the monoaldehyde **3** in 42% yield, and the desired dialdehyde **4** in 13% yield. The attempt to convert the monoaldehyde **3** to dialdehyde **4** *via* Duff rection, succeeded only with a low yield of 3%, which may be explained by the presence of the electron-withdrawing nitro group that reduced the electron density on the aromatic ring.[29a] Nonetheless, after the tedious chromatographic separation, the dialdehyde **4** was isolated and crystalized from ethyl acetate. Single crystal X-ray diffraction measurements revealed its molecular structure (Fig. S1). The dialdehyde **4** was further used as a precursor for the synthesis of the nitronyl-nitroxide radical H_2L **5** in 25% yield, using the Ullman's synthetic pathway.[4,27] The binuclear complexes **1** and **2**, were obtained by reacting cobalt(II) and nickel(II) hexafluoroacetylacetonates with the paramagnetic ligand H_2L in the presence of triethylamine.

Table 1 Crystallographic data and structure refinement parameters for compounds **1** and **2**

Compound	**1-Co**	**2-Ni**
Formula	$C_{62}H_{71}N_8O_{18}F_{24}Cl_3Co$	$C_{62}H_{71}N_8O_{18}F_{24}Cl_3Ni$
Formula weight	1896.47	1896.03
Crystal system	Monoclinic	Monoclinic
Space group	$P2_1/c$	$P2_1/c$
a/Å	12.7086(6)	12.6913(9)
b/Å	34.9069(14)	34.9180(19)
c/Å	18.9598(6)	18.9060(8)
β/°	96.151(4)	95.976(5)
V/Å^3	8362.5(6)	8332.8(8)
Z	4	4
D_c/g cm^{-3}	1.506	1.511
T/K	293(2)	293(2)
μ/mm^{-1}	0.612	0.668
Reflections collected	51 187	37 357
Independent reflection	14 737 [R_{int} = 0.0330]	14 552 [R_{int} = 0.0630]
Observed reflections [$I > 2\sigma(I)$]	9401	7359
Final R indices [$I > 2\sigma(I)$]	0.0775, 0.2323	0.0716, 0.1893
R indices (all data)	0.1117, 0.2637	0.1423, 0.2311
Goodness-of-fit on F^2	1.044	1.020
$\Delta\rho_{min}/\Delta\rho_{max}$ (e Å^{-3})	1.53/−0.97	0.89/−0.65

EPR spectra of the ligand H_2L 5

The EPR spectrum of a nitronyl-nitroxide exhibits in most cases five equidistant lines. In the case of the H_2L **5** ligand, the EPR spectra recorded at 295 K in different solvents show more than five lines due to the spin–spin interactions of the uncoupled electrons (Fig. 1). The literature describes two mechanisms for spin–spin interactions: through space and through bonds in the case of conjugated systems.[40–42] In the case of the H_2L **5** biradical, the mechanism through which spin–spin interactions occurs is through space, these being determined by several factors: the nature of the solvent, the conformation of the molecule, and the temperature. The line intensities assigned to spin–spin interactions are dependent on the nature of the solvent. In more non-polar solvents such as toluene or dichloromethane (DCM) they are more intense and broader (due to the presence of molecular oxygen) than in a polar solvent, such as water. As the structure of the biradical is flexible, the EPR spectra in solution represent a sum of components corresponding to different conformations that bring the two paramagnetic groups at various distances. Therefore, the ratio of spectral line intensities in the experimental EPR spectrum changes

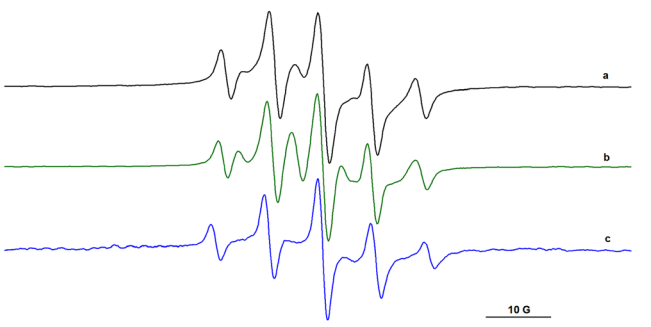

Fig. 1 The EPR spectra of H_2L **5** in: a) toluene, b) dichloromethane, c) water.

depending on the solvent and temperature. The values of the hyperfine splitting constants (a_{N1} = a_{N2}) due to the interaction of the unpaired electron with the nuclei of the two equivalent nitrogen atoms are as follows: 7.45 G (toluene), 7.64 G (DCM) and 8.20 (water).

Spin–spin interactions are defined by spin exchange interaction constant J and the relative value to the hyperfine coupling constant, a_N, influences the shape of the EPR spectrum. As such, in the case of biradicals bearing nitronyl-nitroxide moieties, if $J \gg a_N$, the EPR spectrum in solution consists of 9 lines.[40,41] The spectra displayed in Fig. 1 consists of spectral lines attributed to spin interactions which are present for all solvents, with the particularity that the high-field lines, one attributed to exchange interaction and the other to hyperfine coupling, are not resolved. In the case of the biradical solution in water (Fig. 1c), the intensities of the lines attributed to exchange interactions are very weak and this can be explained by solvation effect and a conformation of the biradical with the two paramagnetic groups at larger distance. At 295 K, the EPR spectrum of the biradical is also very similar to that of a nitronyl-nitroxide monoradical. Therefore, the spectrum of the biradical H_2L **5** in water solution has been recorded at different temperature values in the range 295–333 K (Fig. 2). It can be observed that, by increasing the temperature, the lines assigned to exchange interactions increase in intensity due to the increase in the mobility of the molecule, allowing the two paramagnetic groups to approach each other.

Crystal structures of 1 and 2

The cobalt and nickel complexes, $(Et_3NH)_2[Co_2L(hfac)_4]\cdot CHCl_3$ **1**, $(Et_3NH)_2[Ni_2L(hfac)_4]\cdot CHCl_3$ **2**, are isostructural. Therefore, we describe here only the structure of the nickel derivative (Fig. 3). The crystal structure of **2** consists of anionic dinuclear species, $[Ni_2L(hfac)_4]^{2-}$, triethylammonium cations, Et_3NH^+, and crystallization $CHCl_3$ molecules. Each nickel(II) ion shows an octahedral geometry, being coordinated by four oxygen atoms from the hexafluoroacetylacetonato ($hfac^-$) ligands, and in *cis* positions by the phenoxido and aminoxyl oxygen atoms from the paramagnetic ligand. The two crystallographically independent metal ions are chiral and display Δ (Ni1) and, respectively, Λ (Ni2) configurations. The

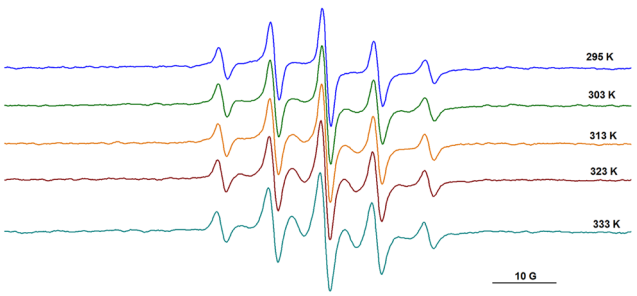

Fig. 2 The EPR spectra of H_2L **5** in water solution recorded in the temperature range 295–333 K.

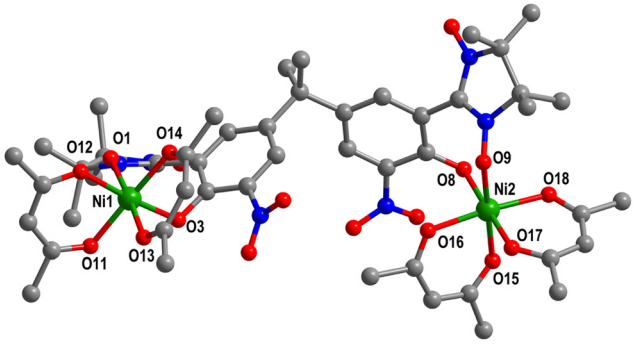

Fig. 3 The X-ray structure of the complex anion **2**, with nickel-green, carbon-grey, oxygen-red, nitrogen-blue and chlorine-yellow; the hydrogen and fluorine atoms have been omitted for clarity.

Ni1–O bonds vary from 2.004(4) to 2.065(5) Å, and the Ni2–O bonds from 2.027(4) to 2.042(4) Å. The bond lengths of the coordinated aminoxyl group to Ni1 (N1–O1 = 1.300(6) Å) and Ni2 (N5–O9 = 1.290(6) Å) are slightly longer than the ones from the uncoordinated NO group (N2–O2 = 1.273(6) and N6–O10 = 1.274(7) Å). The 2-nitrophenol fragments are tilted relative to each other at an angle of 78.6°, with the nitronyl-nitroxide moieties pending in opposite directions. Selected bond distances and angles for compounds **1** and **2** are collected in Table 2. In compound **2** the CF_3 groups are disordered over two crystallographic positions assigned as A (0.411) and B (0.589). For both crystallographic models, the packing diagram reveals a network of intermolecular F···F interactions (2.805–3.285 Å) connecting the dinuclear units at supramolecular level (Fig. S2 and S3). Such interactions are frequently observed with compounds containing C–F bonds, which play an important role in the crystal packing.[43] The diffuse reflectance spectra of the two complexes and of the ligand are presented in Fig. S4. Compound **1** shows, apart from the bands arising from the organic ligands, one band due to the $^3T_1 \rightarrow {}^3T_2$ d–d transition, (1168 nm) while compound **2** displays two bands which are due to the d–d transitions: $^3A_2 \rightarrow {}^3T_2$ (1093 nm) and $^3A_2 \rightarrow {}^3T_1$ (748 nm). The assignments are made assuming the O point group.

Magnetic properties of 1 and 2

Based on the structures of compounds **1** and **2**, we considered them to consist of two metal-radical units that contribute additively to the magnetic susceptibility, without significant magnetic interaction between them. The $\chi_M T$ product for **1** at 300 K is 4.931 $cm^3\ mol^{-1}$ K, (Fig. 4), a value that is smaller than the expected one for two S = 3/2 (Co^{II}) and two S = 1/2 (radical) spins, if the orbital contribution characteristic for the octahedral Co^{II} ion is included (*ca.* 3 $cm^3\ mol^{-1}$ K/Co^{II}, the spin only value being 1.875 $cm^3\ mol^{-1}$ K/Co^{II}). This suggests that the Co^{II} ion and the radical are coupled even at room temperature. By lowering the temperature, $\chi_M T$ decreases slowly to 3.98 $cm^3\ mol^{-1}$ K (100 K), than more and more, reaching 0.410 $cm^3\ mol^{-1}$ K at 2 K. This behavior arises form the magnetic anisotropy of the Co^{II} ion, combined with the antiferromagnetic intercation between each cobalt ion and the

Table 2 Selected bond distances (Å) and angle values (°) in compounds 1 and 2

1-Co		2-Ni	
Distances (Å)			
Co1–O1	2.028(4)	Ni1–O1	2.004(4)
Co1–O3	2.042(3)	Ni1–O3	2.026(3)
Co1–O11	2.098(5)	Ni1–O11	2.007(4)
Co1–O12	2.064(5)	Ni1–O12	2.031(5)
Co1–O13	2.047(4)	Ni1–O13	2.020(5)
Co1–O14	2.067(5)	Ni1–O14	2.065(5)
Co2–O8	2.047(3)	Ni2–O8	2.033(3)
Co2–O9	2.061(3)	Ni2–O9	2.040(4)
Co2–O15	2.081(3)	Ni2–O15	2.038(4)
Co2–O16	2.070(4)	Ni2–O16	2.042(4)
Co2–O17	2.057(4)	Ni2–O17	2.027(4)
Co2–O18	2.074(3)	Ni2–O18	2.034(3)
Angles (°)			
O1 Co1 O3	89.4(2)	O1 Ni1 O3	89.8(2)
O1 Co1 O14	84.5(2)	O1 Ni1 O14	91.8(2)
O1 Co1 O12	174.4(2)	O1 Ni1 O12	84.5(3)
O3 Co1 O14	173.8(3)	O3 Ni1 O14	90.5(3)
O3 Co1 O12	96.1(2)	O3 Ni1 O12	174.1(2)
O3 Co1 O11	90.7(2)	O3 Ni1 O11	92.2(2)
O1 Co1 O11	92.8(2)	O1 Ni1 O11	94.0(2)
O11 Co1 O14	88.8(2)	O11 Ni1 O14	173.5(2)
O11 Co1 O12	86.9(2)	O11 Ni1 O12	90.1(2)
O11 Co1 O13	171.0(2)	O11 Ni1 O13	85.3(2)
O12 Co1 O14	90.0(2)	O12 Ni1 O14	87.6(2)
O13 Co1 O3	93.1(2)	O13 Ni1 O3	95.2(2)
O13 Co1 O1	95.3(2)	O13 Ni1 O1	174.8(3)
O13 Co1 O14	88.2(2)	O13 Ni1 O14	88.6(2)
O13 Co1 O12	84.6(2)	O13 Ni1 O12	90.3(2)
O8 Co2 O9	89.4(2)	O8 Ni2 O9	90.0(2)
O8 Co2 O16	95.2(2)	O8 Ni2 O16	92.0(2)
O8 Co2 O18	90.2(2)	O8 Ni2 O18	89.9(2)
O8 Co2 O15	92.9(2)	O8 Ni2 O15	94.3(2)
O9 Co2 O16	174.6(2)	O9 Ni2 O16	89.4(2)
O9 Co2 O18	97.2(2)	O9 Ni2 O18	95.4(2)
O16 Co2 O18	85.1(2)	O16 Ni2 O18	174.6(2)
O15 Co2 O18	171.7(2)	O15 Ni2 O18	86.0(2)
O15 Co2 O9	90.3(2)	O15 Ni2 O9	175.3(2)
O15 Co2 O16	86.9(2)	O15 Ni2 O16	88.8(2)
O17 Co2 O8	176.9(2)	O17 Ni2 O8	177.3(2)
O17 Co2 O9	87.7(2)	O17 Ni2 O9	87.2(2)
O17 Co2 O16	87.6(2)	O17 Ni2 O16	87.8(2)
O17 Co2 O18	88.8(2)	O17 Ni2 O18	90.3(2)
O17 Co2 O15	88.2(2)	O17 Ni2 O15	88.3(2)

radical moiety. The magnetization *vs.* H/T curves recorded at four temperatures (2; 3; 4; 5 K) (Fig. 4), do not reach saturation, in agreement with the temperature dependence of the $\chi_M T$ product.

The experimental data was fit using the following Hamiltonian:[33,44–46]

$$\hat{H} = -2J\hat{S}_1\hat{S}_2 + \mu_B\left(\alpha\hat{L} + g_1\hat{S}_1 + g_2\hat{S}_2\right)\vec{B} + \alpha\lambda\hat{L}\hat{S}_1 + \alpha^2 B_2^0\left(3\hat{L}_z^2 - \hat{L}^2\right) + \alpha^2\frac{B_2^2}{2}\left(\hat{L}_+^2 - \hat{L}_-^2\right) \quad (1)$$

Here, the parameters are defined as follows: $\alpha = -(3/2)k$ is the orbital reduction factor, k = 1 (fixed) accounts for the covalency contribution of the metal bond; S_1 = 3/2 and S_2 = 1/2 corresponds to the spin of Co^{II} and the radical; L = 1, effective orbital triplet quantum number for Co^{II}; electron g-factor $g_1 = g_2$ = 2.0 (fixed); λ = −170 cm^{-1} (fixed) is the spin–orbit coupling constant. The fitting yielded the following optimized parameters: $B_2(0)$ = 515 ± 5 cm^{-1} is axial distortion factor which represent energy between, $^4A_{2g}$ and ^4E_g;[45] $B_2(2)$ = −7.85 ± 53 represent the rhombohedral distortion and can be assignment to splitting of ^4E_g levels;[46] J = −16.5 ± 0.5 cm^{-1} is the Co^{II}–radical magnetic interaction.

An alternative model that accounts for the pronounced anisotropy of Co^{II} and enables estimation of the magnetic interaction between the Co^{II} center and the radical is the zero-field splitting formalism.[47–51] This approach is particularly suitable for analyzing low-temperature data based on the anisotropic Hamiltonian (2). Fitting the data with this Hamiltonian yielded consistent parameters (D = 22.7 ± 1.0 cm^{-1}; $|E|$ = 5.59 ± 1.0 cm^{-1}; g = 2.10 ± 0.03; J = −13.3 ± 0.4 cm^{-1}) with an exchange constant of comparable magnitude to that obtained from the spin–orbit formalism (see plots in the Fig. S16). It is worth noting the difference in the magnetic interaction of compound **1** compared with a related Co^{II} complex recently reported,[51] which exhibited an antiferromagnetic interaction of approximately −83 cm^{-1} (−2J = −166 cm^{-1}). This discrepancy can be attributed to structural features such as the Co–O bond length of 2.030 Å, the Co–O–N bond angle of 123.0°, and the Co–O–N–C dihedral angle of 67.8°. As it was shown in ref. 51 for the Mn(II)–radical complex, variations in these parameter (particularly the dihedral angle and bond distance) play a decisive role in determining the metal–radical magnetic interaction. In our opinion, this effect becomes even more pronounced when

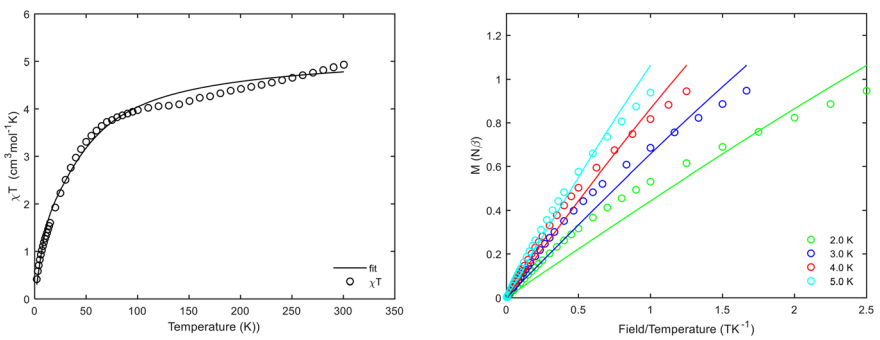

Fig. 4 $\chi_M T$ product *vs.* temperature (left) and magnetization M *vs.* H/T (right) for compound **1** (Co).

the intrinsic magnetic anisotropy of the Co^{II} ion is considered.

The $\chi_M T$ product for **2** at 300 K is 1.845 $cm^3\ mol^{-1}$ K, which is smaller than the expected value of 2.75 $cm^3\ mol^{-1}$ K for two $S = 1$ (Ni^{II}) and two $S = 1/2$ (radical) spins (Fig. 5). The $\chi_M T$ product have a constant decrease with respect of temperature, from 1.85 $cm^3\ mol^{-1}$ at 300 K to 1.17 $cm^3\ mol^{-1}$ K at 100 K reaching a plateau which remains almost constant down to 1.168 $cm^3\ mol^{-1}$ K at 4 K where it exhibits a small decrease to 1.041 $cm^3\ mol^{-1}$ K at 2 K.

The experimental data was fit using the following Hamiltonian,[33]

$$\hat{H} = -2J\hat{S}_1\hat{S}_2 + \mu_B\vec{B}(g_1\hat{S}_1 + g_2\hat{S}_2) + D_1\left(\hat{S}^2_{1,z} - \frac{1}{3}S_1(S_1+1) + E_1\left(\hat{S}^2_{1,x} - \hat{S}^2_{1,y}\right)\right) \quad (2)$$

where $S_1 = 1$, $S_2 = 1/2$, $g_2 = 2.0$ (fixed) resulting the following parameters $g_1 = 2.34 \pm 0.01$, $D_1 = 7.7 \pm 1.6$ cm^{-1}, $|E_1| = 0.27$ cm^{-1} and $J = -147.4 \pm 0.3$ cm^{-1}. The magnetization *vs.* field curves are represented in (Fig. 5): at 2 K, the magnetization reaches the expected value for saturation, taking into account that the g value for Ni^{II} is 2.34, according to the fit to the $\chi_M T$ *vs.* T data.

DFT calculations

Taking into account the structure of the ligand, with two nitronyl-nitroxide paramagnetic centers on the same molecule, well separated by the two phenyl rings connected by the $-C(CH_3)_2-$ group, we consider the magnetic interaction between the two Ni^{II} ions $j_{Ni-Ni} = 0$. Consequently, we performed the calculations for compound **2** considering half of the entire complex system, each fragment consisting in a nitroxide part, a Ni^{II} ion and two hexafluoroacetylacetonato ligands (Fig. S15). For this fragmentation of the ligand we had added at each part a hydrogen atom, in order to avoid the presence of other radical positions.

Starting with the Hamiltonian $H = -2JS_{Ni}S_{rad}$, the J values were calculated using the Ruiz formula,[52] and are displayed in Table 3:

$$2J = (E_{BS} - E_{HS})/(2S_{Ni}S_{Rad} + S_{Rad}) \quad (3)$$

Table 3 Calculated J values (cm^{-1}) for the two fragments

	Lanldz2	TZVP
Fragment 1	−153.13	−164.73
Fragment 2	−171.29	−186.09

The J values obtained for the two fragments, with the B3LYP functional and the lanldz2, and TZVP, basis sets, confirming the antiferromagnetic Ni^{II}–radical interaction, are slightly different, because the two nickel ions are not crystallographically equivalent. The spin densities isosurfaces for the two states (HS and BS) of the first fragment, are presented in Fig. 6. For both states, the spin density is mainly localized on the Ni^{II} ion and to a lower extent on the nitronyl and nitroxide groups.

The experimental and calculated J values for compound **2**, as well as the geometrical parameters associated to the Ni^{II}–NN fragments are close to the ones we found for the cation $[Ni(hfac)_2L']^+$, where L′ is (2-(2-hydroxy-3-methoxy-5-nitrophenyl)-4,4,5,5-tetramethyl-4,5-dihydro-1*H*-imidazol-3-oxide-1-oxyl), a nitronyl-nitroxide ligand derived from nitro-*o*-vanillin (Table 4).[27]

Conclusions

In this paper we have shown that strictly binuclear complexes with nitronyl-nitroxide ligands can be synthesized in a rational way by designing the appropriate dialdehydes decorated with phenolic groups. The crystals structure of one biradical, obtained from 5,5′-(propane-2,2-diyl)bis(2-hydroxy-3-nitrobenzaldehyde), has been solved. The EPR spectra of the biradical recorded in water solutions at various temperatures consist of 9 lines. Two new complexes have been synthesized and characterized, a nickel(II) and a cobalt(II) derivative. The analysis of the packing diagrams of the two crystalline complexes reveals the segregation of the $-CF_3$ groups through F···F intermolecular interactions. The cryomagnetic measurements reveals for both complexes antiferromagnetic 2p–3d exchange interactions. In the case of the nickel derivative, the value of the J parameter is supported by DFT calculation.

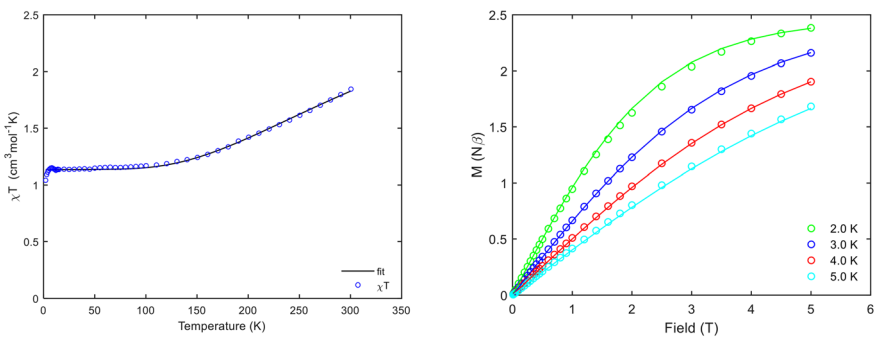

Fig. 5 $\chi_M T$ product *vs.* temperature (left) and magnetization M *vs.* applied field (right) for compound **2** (Ni).

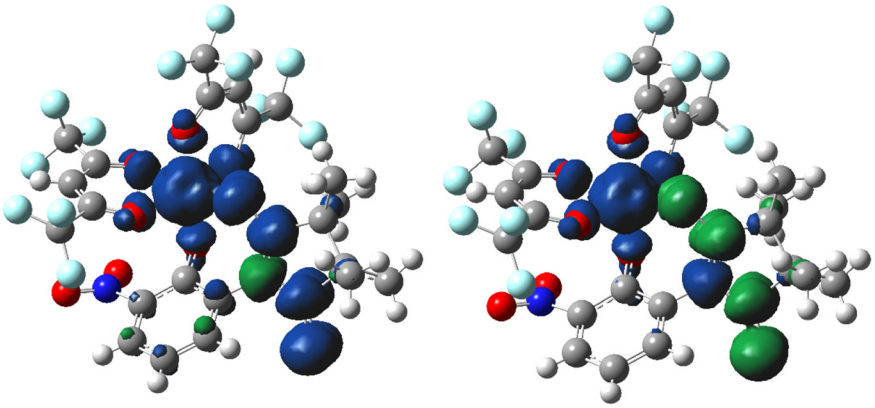

Fig. 6 Spin densities isosurfaces (0.03) of the HS and BS states of the first fragments of the Ni^{II} complex.

Table 4 J values (with respect to $H = -2JS_{Ni}S_{Rad}$) and geometrical parameters for selected mononuclear Ni complex and **2**

	[(Et$_3$NH)[Ni(hfac)$_2$L′]][a]	**2**	
Compound	Ref. 27	(Ni1)	(Ni2)
J_{Ni-NN} (cm^{-1}), experimental	−175.5	−147.4	
J_{Ni-NN} (cm^{-1}), calculated (TZVP)	−200.3	−164.7	−186.1
Ni–O (Å)	2.072(4)	2.004(4)	2.040(4)
Ni–O–N (°)	126.1	124.2	124.9
Ni–O–N–C (°)	58.6	66.2	61.8

[a] L′ = 2-(2-hydroxy-3-methoxy-5-nitrophenyl)-4,4,5,5-tetramethyl-4,5-dihydro-1*H*-imidazol-3-oxide-1-oxyl.

Author contributions

Conceptualization: C. A. S., M. A., G. N., M. H.; formal analysis: C. A. S., G. N., M. H., T. M., G. I., A. H., V. T., M. A.; investigation: C. A. S., G. N., M. H., T. M., G. I., A. H., V. T., M. A.; methodology: C. A. S., M. A., G. N., M. H.; supervision: M. A.; validation: C. A. S., T. M., A. H., V. T.; visualization: C. A. S., T. M., G. N., M. H.; writing – original draft: C. A. S., G. N., M. H., T. M., G. I., M. A.; writing – review & editing: C. A. S., G. N., M. H., T. M., G. I., A. H., V. T., M. A.

Conflicts of interest

There are no conflicts to declare.

Data availability

Supplementary information is available. See DOI: **https://doi.org/10.1039/D5CE00795J**.

Relevant experimental and characterization data been included within the article and as part of ESI.

Acknowledgements

The financial support from European Union through NextGeneration EU-PNRR-III-C9-2022-I8 program (contract no. 760230) is gratefully acknowledged. Authors are grateful to S. Nica (ICOS, Bucharest) for insightful advice regarding the synthesis of aldehydes and M. Răducă (ICOS, Bucharest) for X-ray powder diffraction measurements.

References

1 (*a*) A. Caneschi, D. Gatteschi, R. Sessoli and P. Rey, *Acc. Chem. Res.*, 1989, **22**, 392–398; (*b*) D. Luneau and P. Rey, *Coord. Chem. Rev.*, 2005, **249**, 2591–2611; (*c*) S. Demir, I.-R. Jeon, J. R. Long and T. D. Harris, *Coord. Chem. Rev.*, 2015, **289–290**, 149–176; (*d*) X. Meng, W. Shi and P. Cheng, *Coord. Chem. Rev.*, 2019, **378**, 134–150; (*e*) D. Luneau, *Eur. J. Inorg. Chem.*, 2020, **2020**, 597–604; (*f*) M. G. F. Vaz and M. Andruh, *Coord. Chem. Rev.*, 2021, **427**, 213611; (*g*) H. Tanaka, D. Shiomi, T. Ise, K. Sato and T. Takui, *CrystEngComm*, 2007, **9**, 767–771; (*h*) M. Zhu, D. Lou, X. Deng, L. Zhang, W. Zhanga and Y. Lü, *CrystEngComm*, 2018, **20**, 2583–2592; (*i*) J. Sun, M. Chen, Y. Li, X. Liu, X. Fu, L. Hea and C. Jin, *CrystEngComm*, 2022, **24**, 8160–8167; (*j*) Y. Zhou, J. Xie, X. Huang, C. Jin, Y. Ma and L. Li, *CrystEngComm*, 2025, **27**, 1120–1127.

2 A. Caneschi, D. Gatteschi, N. Lalioti, C. Sangregorio, R. Sessoli, G. Venturi, A. Vindigni, A. Rettori, M. G. Pini and M. A. Novak, *Angew. Chem., Int. Ed.*, 2001, **40**, 1760–1763.

3 (*a*) M. G. F. Vaz, R. A. Allão Cassaro, H. Akpinar, J. A. Schlueter, P. M. Lahti and M. Novak, *Chem. – Eur. J.*, 2014, **20**, 5460–5467; (*b*) X. Liu, X. Feng, K. R. Meihaus, X.

Meng, Y. Zhang, L. Li, J.-L. Liu, W. Shi, Y.-Q. Zhang, P. Cheng and J. R. Long, *Angew. Chem., Int. Ed.*, 2020, **59**(26), 10610–10618; (*c*) T. A. Costa, M. Răducă, J. C. Rocha, M. A. Novak, R. A. A. Cassaro, M. Andruh and M. G. F. Vaz, *Inorg. Chem. Front.*, 2025, **12**, 1393–1402.

4 E. F. Ullman, J. H. Osiecki, D. G. B. Boocock and R. Darcy, *J. Am. Chem. Soc.*, 1972, **94**, 7049–7059.

5 Y.-L. Gao, Y. Wang, L. Gao, J. Li, Y. Wang and K. Inoue, *ACS Omega*, 2022, **7**, 10022–10028.

6 (*a*) A. Caneschi, P. Chiesi, L. David, F. Ferraro, D. Gatteschi and R. Sessoli, *Inorg. Chem.*, 1993, **32**, 1445–1453; (*b*) Y.-L. Gao, P. Gao, Y. Gong and G. Ren, *J. Chem. Res.*, 2021, **45**, 590–595; (*c*) Y.-L. Gao, S. Nishihara, T. Suzuki, K. Umeo, K. Inoue and M. Kurmoo, *Dalton Trans.*, 2022, **51**, 6682–6686; (*d*) S. Grenda, M. Beau and D. Luneau, *Molecules*, 2022, **27**, 3218.

7 L. Xi, H. Li, J. Sun, Y. Ma, J. Tang and L. Li, *Inorg. Chem.*, 2020, **59**, 443–451.

8 S. Y. Zhou, X. Li, T. Li, L. Tian, Z. Y. Liu and X. G. Wang, *RSC Adv.*, 2015, **5**, 17131–17139.

9 H. Li, J. Sun, M. Yang, Z. Sun, J. Xie, Y. Ma and L. Li, *New J. Chem.*, 2017, **41**, 10181–10188.

10 J. Sun, Q. Wu, J. Lu, P. Jing, Y. Du and L. Li, *Dalton Trans.*, 2020, **49**, 17414–17420.

11 H. Li, L. Xi, L. Zhai and Y. Niu, *J. Mol. Struct.*, 2019, **1196**, 653–657.

12 P. Jing, L. Xi, J. Lu, J. Han, X. Huang, C. Jin, J. Xie and L. Li, *Chem. – Asian J.*, 2021, **16**, 793–800.

13 H. Li, J. Sun, M. Yang, Z. Sun, J. Tang, Y. Ma and L. Li, *Inorg. Chem.*, 2018, **57**, 9757–9765.

14 L. Xi, C.-Y. Jin, H.-W. Song, X.-T. Wang, L.-C. Li and J.-P. Sutter, *Dalton Trans.*, 2022, **51**, 6955–6963.

15 J. Sun, J. Xie, L. Li and J.-P. Sutter, *Inorg. Chem. Front.*, 2020, **7**, 1949–1956.

16 J. Han, C. Jin, X. Wang, X. Huang, H. Song, J. Xie and L. Li, *Dalton Trans.*, 2023, **52**, 6853–6859.

17 H. Song, C. Jin, X. Wang, J. Xie, Y. Ma, J. Tang and L. Li, *Dalton Trans.*, 2024, **53**, 10007–10017.

18 D. Zhang, W. Liu, W. Xu, X. Jin and D. Zhu, *Inorg. Chim. Acta*, 2001, **318**, 84–88.

19 D. Zhang, W. Liu, Z. Shuai, H. Hu, W. Xu and D. Zhu, *Synth. Met.*, 2003, **113–134**, 601–603.

20 X. Deng, S. Ma, M. Zhu, L. Zhang and Y. Lv, *New J. Chem.*, 2020, **44**, 7858–7864.

21 D. Luneau, F. M. Romero and R. Ziessel, *Inorg. Chem.*, 1998, **37**, 5078–5087.

22 C. Stroh and R. Ziessel, *Chem. Commun.*, 2002, 1916–1917.

23 E. Tretyakov, S. Fokin, G. Romanenko, V. Ikorskii, S. Vasilevsky and V. Ovcharenko, *Inorg. Chem.*, 2006, **45**, 3671–3678.

24 C.-C. Xia, W.-J. Ji, X.-Y. Zhang, H. Miao, Y.-Q. Zhang and X.-Y. Wang, *Dalton Trans.*, 2022, **51**, 12362–12372.

25 C. Wang, Y. Ma, X. Yang, S. Yan and D. Liao, *Chin. J. Chem.*, 2010, **28**, 1593–1599.

26 X.-T. Wang, X.-H. Huang, H.-W. Song, Y. Ma, L.-C. Li and J.-P. Sutter, *Molecules*, 2023, **28**, 2514.

27 C. A. Spinu, C. Pichon, G. Ionita, T. Mocanu, S. Calancea, M. Raduca, J.-P. Sutter, M. Hillebrand and M. Andruh, *J. Coord. Chem.*, 2021, **74**, 279–293.

28 (*a*) B. Murrell, *McNair Scholars J.*, 2006, **10**, 10; (*b*) S. Babu, C. Pathak, S. Uppu, C. Jones, F. R. Fronczek and R. M. Uppu, *Acta Crystallogr., Sect. E: Struct. Rep. Online*, 2011, **67**, 2556–2557.

29 (*a*) L. F. Lindoy, G. V. Meehan and N. Svenstrup, *Synthesis*, 1998, **7**, 1029–1032; (*b*) E. Asato, M. Chinen, A. Yoshino, Y. Sakata and K. Sugiura, *Chem. Lett.*, 2000, **29**, 678–679; (*c*) M. W. Schneider, I. M. Oppel and M. Mastalerz, *Chem. – Eur. J.*, 2012, **18**, 4156–4160.

30 O. Kahn, *Molecular Magnetism*, VCH Publishers, Inc, 1993.

31 P. Pascal, *Ann. Chim. Phys.*, 1910, **19**, 5.

32 G. A. Bain and J. F. Berry, *J. Chem. Educ.*, 2008, **85**(4), 532–536.

33 N. F. Chilton, R. P. Anderson, L. D. Turner, A. Soncini and K. S. Murray, *J. Comput. Chem.*, 2013, **34**(13), 1164–1175.

34 D. R. Duling, *PEST Winsim, version 0.96*, National Institute of Environmental Health Sciences, Triangle Park, NC, 1996.

35 (*a*) G. M. Sheldrick, Crystal structure refinement with SHELX, *Acta Crystallogr., Sect. C: Struct. Chem.*, 2015, **71**, 3–8; (*b*) G. M. Sheldrick, SHELXT – Integrated space-group and crystal-structure determination, *Acta Crystallogr., Sect. A: Found. Adv.*, 2015, **71**, 3–8.

36 M. J. Frisch, G. W. Trucks, H. B. Schlegel, G. E. Scuseria, M. A. Robb, J. R. Cheeseman, G. Scalmani, V. Barone, B. Mennucci, G. A. Petersson, H. Nakatsuji, M. Caricato, X. Li, H. P. Hratchian, A. F. Izmaylov, J. Bloino, G. Zheng, J. L. Sonnenberg, M. Hada, M. Ehara, K. Toyota, R. Fukuda, J. Hasegawa, M. Ishida, T. Nakajima, Y. Honda, O. Kitao, H. Nakai, T. Vreven, J. A. Montgomery, J. E. Peralta, F. Ogliaro, M. Bearpark, J. J. Heyd, E. Brothers, K. N. Kudin, V. N. Staroverov, R. Kobayashi, J. Normand, K. Raghavachari, A. Rendell, J. C. Burant, S. S. Iyengar, J. Tomasi, M. Cossi, N. Rega, J. M. Millam, M. Klene, J. E. Knox, J. B. Cross, V. Bakken, C. Adamo, J. Jaramillo, R. Gomperts, R. E. Stratmann, O. Yazyev, A. J. Austin, R. Cammi, C. Pomelli, J. W. Ochterski, R. L. Martin, K. Morokuma, V. G. Zakrzewski, G. A. Voth, P. Salvador, J. J. Dannenberg, S. Dapprich, A. D. Daniels, O. Farkas, J. B. Foresman, J. V. Ortiz, J. Cioslowski and D. J. Fox, *GAUSSIAN 09, Revision C.01*, Gaussian, Inc., Wallingford, CT, 2009.

37 A. D. Becke, *J. Chem. Phys.*, 1993, **98**, 5648–5652.

38 T. H. Dunning Jr. and P. J. Hay, in *Modern Theoretical Chemistry*, ed. H. F. Schaefer III, Plenum, New York, 1977, vol. 3, pp. 1–28.

39 F. Weigend and R. Ahlrichs, *Phys. Chem. Chem. Phys.*, 2005, **7**, 3297–3305.

40 I. A. Zayakin, I. V. Kurganskii, A. Keerthi, M. Baumgarten, A. A. Dmitriev, N. P. Gritsan, S. E. Tolstikov, R. Z. Sagdeev, A. A. Korlyukov, E. V. Tretyakov and M. V. Fedin, *Appl. Magn. Reson.*, 2025, **56**, 125–135.

41 R. Rausch, A.-M. Krause, I. Krummenacher, H. Braunschweig and F. Würthner, *J. Org. Chem.*, 2021, **86**, 2447–2457.
42 D. Wang, Y. Ma, B. Wolf, A. I. Kokorin and M. Baumgarten, *J. Phys. Chem. A*, 2018, **122**(2), 574–581.
43 (*a*) O. J. Dautel, M. Fourmigué, E. Canadell and P. Auban-Senzier, *Adv. Funct. Mater.*, 2002, **12**, 693–698; (*b*) S. S. Batsanov, *Inorg. Mater.*, 2001, **37**, 871–885; (*c*) G. V. Janjić, S. T. Jelić, N. P. Trišović, D. M. Popović, I. S. Đorđević and M. K. Milčić, *Cryst. Growth Des.*, 2020, **20**, 2943–2951; (*d*) A. A. Apostol, R. Oestreich, C. Maxim, C. Romanitan, M. Badea, C. Janiak and M. Andruh, *Cryst. Growth Des.*, 2023, **23**, 3740–3746.
44 G. K. Gransbury, M. E. Boulon, R. A. Mole, R. W. Gable, B. Moubaraki, K. S. Murray, L. Sorace, A. Soncini and C. Boskovic, *Chem. Sci.*, 2019, **10**(38), 8855–8871.
45 F. Lloret, M. Julve, J. Cano, R. Ruiz-García and E. Pardo, *Inorg. Chim. Acta*, 2008, **361**(12–13), 3432–3445.
46 A. V. Palii, D. V. Korchagin, E. A. Yureva, A. V. Akimov, E. Ya. Misochko, G. V. Shilov, A. D. Talantsev, R. B. Morgunov, S. M. Aldoshin and B. S. Tsukerblat, *Inorg. Chem.*, 2016, **55**(19), 9696–9706.
47 L. Rigamonti, N. Bridonneau, G. Poneti, L. Tesi, L. Sorace, D. Pinkowicz, J. Jover, E. Ruiz, R. Sessoli and A. Cornia, *Chem. – Eur. J.*, 2018, **24**, 8857–8868.
48 A. Z. Lekuona, A. L. Gereka, M. M. Q. Moreno, A. J. Mota, I. F. D. Ortega, H. Nojiri, J. Krzystek, J. M. Seco and E. Colacio, *Inorg. Chem.*, 2023, **62**(49), 20030–20041.
49 G. Novitchi, S. Jiang, S. Shova, F. Rida, I. Hlavicka, M. Orlita, W. Wernsdorfer, R. Hamze, C. Martins, N. Suaud, N. Guihery, A. L. Barra and C. Train, *Inorg. Chem.*, 2017, **56**(24), 14809–14822.
50 G. Novitchi, S. Shova and C. Train, *Inorg. Chem.*, 2022, **61**(43), 17037–17048.
51 C. A. Spinu, D. O. T. A. Martins, T. Mocanu, M. Hillebrand, J.-P. Sutter, F. Tuna and M. Andruh, *Magnetochemistry*, 2024, **10**, 86.
52 E. Ruiz, J. Cano, S. Alvarez and P. Alemany, *J. Comput. Chem.*, 1999, **20**, 1391–1400.

